Monthly Notices of the ROYAL ASTRONOMICAL SOCIETY

MNRAS **458,** 3466–3477 (2016) doi:10.1093/mnras/stw532
Advance Access publication 2016 March 10

Nitrogen and oxygen abundances in the Local Universe

F. Vincenzo,[1,2]★ F. Belfiore,[3,4] R. Maiolino,[3,4] F. Matteucci[1,2,5] and P. Ventura[6]

[1]*Dipartimento di Fisica, Sezione di Astronomia, Università di Trieste, via G.B. Tiepolo 11, I-34100 Trieste, Italy*
[2]*INAF, Osservatorio Astronomico di Trieste, via G.B. Tiepolo 11, I-34100 Trieste, Italy*
[3]*Cavendish Laboratory, University of Cambridge, 19 J. J. Thomson Avenue, Cambridge CB3 0HE, UK*
[4]*Kavli Institute for Cosmology, University of Cambridge, Madingley Road, Cambridge CB3 0HA, UK*
[5]*INFN, Sezione di Trieste, Via Valerio 2, I-34100 Trieste, Italy*
[6]*INAF, Osservatorio Astronomico di Roma, via Frascati 33, I-0004 Monte Porzio Catone (RM), Italy*

Accepted 2016 March 2. Received 2016 March 1; in original form 2015 November 19

ABSTRACT

We present chemical evolution models aimed at reproducing the observed (N/O) versus (O/H) abundance pattern of star-forming galaxies in the Local Universe. We derive gas-phase abundances from Sloan Digital Sky Survey (SDSS) spectroscopy and a complementary sample of low-metallicity dwarf galaxies, making use of a consistent set of abundance calibrations. This collection of data clearly confirms the existence of a plateau in the (N/O) ratio at very low metallicity, followed by an increase of this ratio up to high values as the metallicity increases. This trend can be interpreted as due to two main sources of nitrogen in galaxies: (i) massive stars, which produce small amounts of pure primary nitrogen and are responsible for the (N/O) ratio in the low-metallicity plateau; (ii) low- and intermediate-mass stars, which produce both secondary and primary nitrogen and enrich the interstellar medium with a time delay relative to massive stars, and cause the increase of the (N/O) ratio. We find that the length of the low-metallicity plateau is almost solely determined by the star formation efficiency, which regulates the rate of oxygen production by massive stars. We show that, to reproduce the high observed (N/O) ratios at high (O/H), as well as the right slope of the (N/O) versus (O/H) curve, a differential galactic wind – where oxygen is assumed to be lost more easily than nitrogen – is necessary. No existing set of stellar yields can reproduce the observed trend without assuming differential galactic winds. Finally, considering the current best set of stellar yields, a bottom-heavy initial mass function is favoured to reproduce the data.

Key words: stars: abundances – ISM: abundances – ISM: evolution – galaxies: abundances – galaxies: evolution – galaxies: ISM.

1 INTRODUCTION

The self-regulation of star formation in galaxies by gas accretion and galactic outflows is a fundamental ingredient in the modern framework of galaxy evolution. Both the analysis of large galaxy surveys and the direct observation of high-velocity clouds (e.g. Fraternali et al. 2002; Oosterloo, Fraternali & Sancisi 2007; Heald et al. 2011; Gentile et al. 2013), as well as hydrodynamical simulations (Prochaska & Wolfe 2009; Faucher-Giguère, Kereš & Ma 2011; van de Voort et al. 2011; Dekel et al. 2013; Fraternali et al. 2015) point towards the need for continuous accretion of pristine gas on to galaxies (see also Fraternali & Binney 2008; Putman, Peek & Joung 2012). Moreover, historically, the so-called G-dwarf problem (van den Bergh 1962; Schmidt 1963; Tinsley 1980) was solved by relaxing the hypothesis of a closed-box evolution of the solar neighbourhood and allowing the accretion of pristine gas on to the disc, which acts in diluting the abundances; in this way, one can reconcile the predicted frequency of metal-poor Galactic disc stars (which are too many in the framework of the simple closed-box model) with the observed one. Large-scale galactic winds and outflows are also necessary to reproduce the overall properties of the observed galaxy population and to match the observed chemical enrichment of the intergalactic medium (IGM; see, for example, Erb 2008; Finlator & Davé 2008; Fabian 2012; Hopkins, Quataert & Murray 2012). Several observations of galactic outflows in the literature have demonstrated the ubiquity of the outflow phenomenon, both locally and at high redshift (see, for example, Pettini et al. 2001; Bolatto et al. 2013; Cicone et al. 2014, 2015; Geach et al. 2014; Erb 2015), however, understanding their impact on galaxy properties over cosmic time remains a daunting task.

Since metals are a direct product of star formation in galaxies, chemical abundances are a powerful probe of the feedback processes driving the evolution of galaxies. Oxygen occupies a key role in this

★ E-mail: vincenzo@oats.inaf.it

type of studies, since its gas-phase abundance can be inferred from strong nebular lines easily observed in the optical wavelength range in the low-redshift Universe. Since oxygen is the most common metal by mass, its abundance is also an excellent proxy for the total metallicity of the gas. Moreover, since oxygen is mostly produced by massive stars, dying as core-collapse supernovae (SNe), its enrichment is relatively simple to model and does not require, to first approximation, taking into account the effect of stellar lifetimes (under the so-called instantaneous recycling approximation, IRA).

The study of the relation between oxygen abundance and other fundamental galaxy parameters like stellar mass (Lequeux et al. 1979; Tremonti et al. 2004), star formation rate (SFR; Mannucci et al. 2010; Andrews & Martini 2013), gas content (Bothwell et al. 2013; Hughes et al. 2013) and environment (Pasquali et al. 2010; Peng & Maiolino 2014) has paved the way to the development of a new generation of chemical evolution models (Davé, Finlator & Oppenheimer 2012; Lilly et al. 2013; Peng & Maiolino 2014; Lu, Blanc & Benson 2015; Belfiore, Maiolino & Bothwell 2016), which succeed, to various extents, at reproducing the general trends observed in the data with cosmological inflow rates and various simple outflow prescriptions.

Since different chemical elements are released in the interstellar medium (ISM) on different time-scales, the study of abundance ratios of some key elements can provide tighter constraints on the star formation and gas flow history of a system. For example, large galaxy surveys have demonstrated that the [O/Fe] ratios in elliptical galaxies are consistent with the paradigm requiring these objects to form stars vigorously over a short time-scale at high redshift (Matteucci 1994; Bernardi et al. 2003; Pipino & Matteucci 2004; Thomas et al. 2005, 2010). Moreover, detailed analysis of chemical abundance ratios of *n*-capture, α- and iron-peak elements in individual stars in the Milky Way (MW) have been instrumental in showing that the various components of our Galaxy (halo, bulge, thick and thin disc) have had different chemical evolution histories with respect to each other (see, for example, Pagel 2009; Matteucci 2001, 2012).

In the context of star-forming galaxies, strong nebular lines in the optical range allow reliable measurement of the (N/O) abundance ratio when both the [O II] $\lambda\lambda$3726, 3729 and [N II] $\lambda\lambda$6548, 6584 doublets are measured. The (N/O) abundance ratio has been studied by several authors (Vila-Costas & Edmunds 1992; Thuan, Izotov & Lipovetsky 1995; Henry, Edmunds & Köppen 2000; Chiappini, Romano & Matteucci 2003; Chiappini, Matteucci & Ballero 2005; Pérez-Montero & Contini 2009; Pérez-Montero et al. 2013; Belfiore et al. 2015), since it is a promising tool to shed light on the relative role of pristine gas inflows and outflows, which appear degenerate when only the abundance of one chemical element is traced (see Köppen & Hensler 2005, but also the discussion in the appendix of Belfiore et al. 2016).

Unlike oxygen, nitrogen is a chemical element mostly produced by low- and intermediate-mass stars (LIMS), with the nucleosynthetic yields depending on metallicity in a complex fashion. In particular, a stellar generation can release into the galaxy ISM both primary and secondary N. The secondary N component increases with metallicity, being a product of the CNO cycle and formed at expenses of the C and O already present in the star. Concerning LIMS, the primary N component is produced during the third dredge-up, occurring along the asymptotic giant branch (AGB) phase, if nuclear burning at the base of the convective envelope is efficient (Renzini & Voli 1981). The latter is particularly important for very metal-poor LIMS, which would not be capable otherwise of synthesizing significant amounts of secondary N. On the other hand, the computation of the N stellar yields for massive stars still suffers of large uncertainty, especially at very low metallicity, and none of the current existing stellar evolutionary codes is able to provide the right amount of primary N which is needed to reproduce the observed (N/O) plateau at very low metallicities.

All the aforementioned complications prevent one from using IRA and a constant yield for the study of nitrogen abundances in galaxies, and have prevented the community so far from taking full advantage of the large nitrogen abundance data sets now available both through large spectroscopic surveys of local (like SDSS; York et al. 2000, or GAMA; Driver et al. 2011) and high-redshift (e.g. zCOSMOS; Lilly et al. 2009) galaxies.

In this work, we critically revise the different assumptions affecting the interpretation of the (N/O) versus (O/H) abundance patterns, making use of a large data set of star-forming galaxies from the Sloan Digital Sky Survey (SDSS), complemented by data from metal-poor dwarf galaxies to explore the low-metallicity regime. While considerable uncertainties still persist in some of the basic model parameters (nitrogen yields, stellar initial mass function, IMF) we aim here at setting new constraints on pristine gas inflows and the models of outflows.

The paper is structured as follows. In Section 2, we present the data set used in this work for the (N/O) versus (O/H) abundance diagram. In Section 3, we summarize the current knowledge about the nucleosynthetic origin of nitrogen in stars. In Section 4, we describe the basic equations and the assumptions of the numerical model of chemical evolution adopted in this work. Our results are presented in Section 5 and 6; in particular, in Section 5, we focus on the results of our models for the (N/O) versus (O/H) abundance pattern of the ensemble of the SDSS galaxies; in Section 6, we present the results of our models for the low-metallicity plateau, which a complementary sample of metal-poor, diffuse and star-forming dwarf galaxies exhibit in the (N/O) versus (O/H) diagram. Finally, in Section 7, we end with our conclusions.

2 OVERVIEW OF THE DATA

In order to study the characteristic gas-phase oxygen and nitrogen abundances in local galaxies, we make use of the data from SDSS Data Release 7 (Abazajian et al. 2009, DR7) and the emission line fluxes, stellar masses and SFR estimates presented in the MPA-JHU catalogue[1] (Kauffmann et al. 2003; Brinchmann et al. 2004; Tremonti et al. 2004) released as part of DR 8 (Aihara et al. 2011).

We select galaxies to have $0.023 < z < 0.3$ and S/N > 3 on the following emission lines: [O II] $\lambda\lambda$3726, 28; [O III] λ5007; H β; H α; [N II] λ6584, and [S II] $\lambda\lambda$6717, 31. We use the standard Baldwin–Philipps–Terlevich diagram (Baldwin, Phillips & Terlevich 1981; Veilleux & Osterbrock 1987; Kauffmann et al. 2003) to exclude sources where the gas ionization is not dominated by star formation, since available metallicity calibrations are only tailored to star-forming regions. In this work, we use the [O III]/H β versus [S II]/H α diagnostic diagram and the demarcation curve of Kewley et al. (2001). We do not make use of the popular [O III]/Hβ versus [N II]/Hα to avoid a bias against nitrogen enriched H II regions (Belfiore et al. 2015; Sánchez et al. 2015).

Emission line fluxes are then corrected for dust extinction using the Balmer decrement and the Calzetti (2001) reddening curve with $R_V = 4.05$. The theoretical value for the Balmer line ratio is taken

[1] The MPA-JHU catalogue is available online at https://www.sdss3.org/dr8/spectro/galspec.php

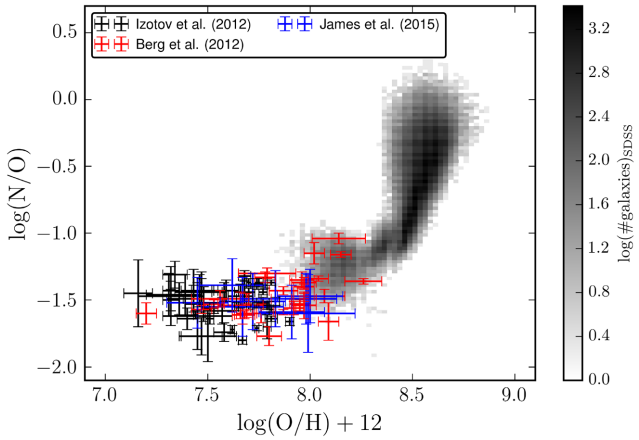

Figure 1. In this figure, the SDSS data sample for the (N/O) versus (O/H) abundance pattern (density plot in grey scale) is compared with a data sample which includes the (N/O) and (O/H) abundances as observed in blue, diffuse star-forming dwarf galaxies by Berg et al. (2012, red data), Izotov, Thuan & Guseva (2012, black data) and James et al. (2015, blue data).

from Osterbrock & Ferland (2006), assuming case B recombination ($H\alpha/H\beta = 2.87$). We note that the use of extinction curves of Cardelli, Clayton & Mathis (1989) or Charlot & Fall (2000) yield very similar results for the wavelength range considered in this work.

Inferring gas-phase oxygen abundance from strong nebular line ratios is a difficult problem, since the line ratios depend not only on ionic abundances, but also on other parameters, such as ionization parameter, density and hardness of ionization field. It is well known in the literature that different oxygen abundance calibrations based on strong nebular lines can lead to systematic discrepancies of up to 0.6 dex (Kewley & Ellison 2008; López-Sánchez et al. 2012; Blanc et al. 2015). In particular, strong line calibrations based on an extrapolation to high metallicity of abundances measured with the τ_e method (which makes use of the faint oxygen auroral line [O III] λ4363 to directly infer the electron temperature of the nebula) generally lead to lower abundances than calibrations based on photoionization models.

Moreover, several metallicity calibrators make use of the nitrogen line fluxes, thus implicitly assuming that the relationship between the (N/O) ratio and metallicity varies monotonically with oxygen abundance.

In this work, we infer the oxygen and nitrogen abundances using the self-consistent framework presented in Pilyugin, Vílchez & Thuan (2010), which calibrates various strong line ratios through the electron temperature method. An alternative calibration taking both oxygen and nitrogen abundance into account has been recently presented in Pérez-Montero (2014).

In order to sample the low-metallicity regime, which is poorly populated in SDSS, we make use of the data from Izotov et al. (2012), Berg et al. (2012) and James et al. (2015) for a collection of blue, diffuse and star-forming dwarf galaxies. We note that the abundances reported by Izotov et al. (2012), Berg et al. (2012) and James et al. (2015) correspond to the chemical abundances as measured using the direct method and hence should fall on to the same scale of chemical abundances we inferred from the SDSS data with the adopted calibration.

In Fig. 1, we show the trend of the observed (N/O) ratios as a function of the (O/H) abundances. The density plot in grey scale represents the abundance pattern as observed in the ensemble of the SDSS galaxies, whereas the data with error bars represent the compilation of star-forming dwarf galaxies from Berg et al. (2012), Izotov et al. (2012) and James et al. (2015). The latter data extend towards lower (O/H) abundances than the SDSS data and clearly exhibits the well-known low-metallicity plateau. The SDSS data show an abrupt change of the slope at oxygen abundances higher than $12 + \log(O/H) \sim 8.4$ dex.

2.1 Estimating the dust depletion

Oxygen abundance calibrations based on nebular lines only trace the oxygen abundance of the gaseous phase of the ISM. However, chemical elements in real galaxies are partially depleted on to dust grains. Since chemical evolution models only predict the total metallicity, depletion on to dust grains must be taken into account when comparing models with our data. From an observational point of view, the dust content can differ among galaxies of different metallicity and SFR (da Cunha et al. 2010; Fisher et al. 2014; Hjorth, Gall & Michałowski 2014). In the framework of chemical evolution studies, the most important physical process affecting the dust cycle in galaxies is the star formation history, which regulates the main feedback processes responsible for the dust production and destruction and hence the run of the galaxy dust-to-gas ratio with metallicity (Wang 1991; Dwek 1998; Lisenfeld & Ferrara 1998; Edmunds 2001; Calura, Pipino & Matteucci 2008; Dwek & Cherchneff 2011; Feldmann 2015).

In the literature, a mean oxygen depletion[2] of $D(O) \approx -0.1$ dex is often assumed (see also Whittet 2003, 2010; Jenkins 2009). Although oxygen depletion is likely to have a dependance on metallicity (differential depletion), for simplicity, we do not consider this effect in this work. Although Jenkins (2009) suggests an average nitrogen depletion of ~ -0.1 dex, the large uncertainty in this estimate means that nitrogen is also consistent with zero depletion. Indeed most of the studies indicate that nitrogen is not a refractory element and does not deplete on to grains even in the densest molecular clouds (e.g. Meyer, Cardelli & Sofia 1997; Caselli et al. 2002). In light of this, in our work, we do not consider any nitrogen depletion on to dust. While the depletion corrections applied in this work are rather arbitrary, none of our conclusions depend on the exact values of the depletion factors.

3 THE NUCLEOSYNTHETIC ORIGIN OF NITROGEN

According to its mass and initial chemical composition, each star pollutes the ISM with different amounts of a given chemical element. Since stellar lifetimes primarily depend upon the stellar mass, each chemical element is expected to enrich the ISM of galaxies on different typical time-scales.

3.1 Primary and secondary nucleosynthetic products

A fundamental aspect to take into account in chemical evolution models is the nature of the physical processes which give rise to the production of the various chemical elements in stars. In particular:

(i) If a sequence of nuclear reactions involves as initial seed only the H and He present in the gas mixture of the star at its birth,

[2] The depletion factor $D(X)$ is the logarithmic decrement between the observed abundance of a chemical element and its predicted total abundance, $A(X)$, namely $D(X) \equiv \log (N_X/N_H)_{obs} - A(X)$.

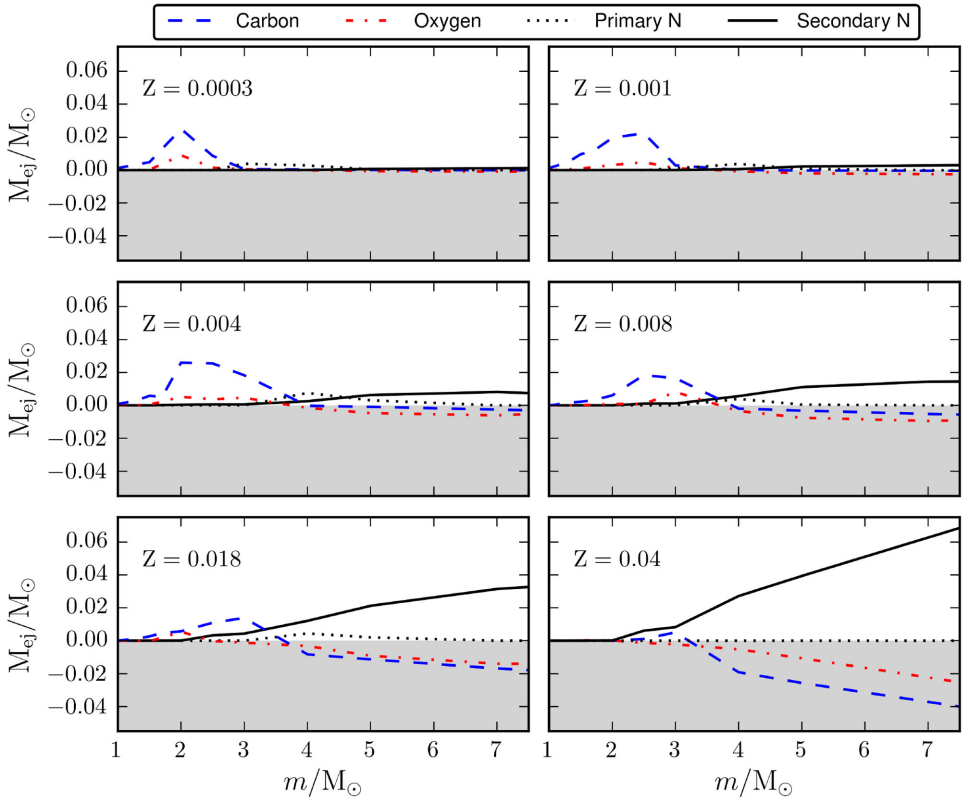

Figure 2. In this figure, we show the Ventura et al. (2013) stellar yields of LIMS for carbon (dashed blue line), oxygen (dash–dotted red line), primary nitrogen (dotted black line) and secondary nitrogen (solid black line), as computed at $Z = 0.0003, 0.001, 0.004, 0.008, 0.018$, and 0.04. The various quantities do not include the amount of ejected mass which was initially present in the star and has not been nuclearly processed; so the finding of negative values for the stellar yields means that the final total ejected amount of the generic element X is smaller than the one which was initially present in the star at its birth and has been later ejected into the ISM without any nuclear processing.

then the nucleosynthetic products of that sequence do not depend upon the initial stellar metallicity. The chemical products of these reactions are then named primary elements.

(ii) If the presence of metals in the initial gas mixture of the star is necessary for some nuclear reactions to occur, then the nucleosynthetic products of those nuclear reactions depend on the metallicity. These chemical products are named secondary elements.

In modern chemical evolution studies, the importance of distinguishing between the secondary and primary nature has been simplified for most of the chemical elements, since their yields are computed as a function of the initial metallicity. Nevertheless, for chemical elements like nitrogen, which have both a primary and secondary origin (see, for example, Edmunds & Pagel 1978; Alloin et al. 1979; Renzini & Voli 1981; Matteucci 1986; Gavilán, Mollá & Buell 2006; Mollá et al. 2006), it can be conceptually useful to separate the two components, even in the presence of yields computed for different metallicities.

3.2 The production of nitrogen in the CNO cycle

Nitrogen is mainly produced during the CNO cycle, whose main branch consists in a series of p-captures and β^+ decays starting from an atom of ^{12}C and converting four protons into a nucleus of He (with two e^+ and two ν_e as byproducts). Since the inner reaction ^{14}N(p, γ)^{15}O proceeds with the slowest rate among the other in the sequence, when the equilibrium condition is reached (namely, when the rate of production of each CNO nucleus equals its rate of destruction), the ultimate effect of the CNO cycle is to convert most of the CNO isotopes into ^{14}N. The origin of the initial ^{12}C seed in the CNO cycle is a discriminating factor. In fact, if the atom of ^{12}C was initially present in the gas mixture from which the star originated, then the synthesized nitrogen behaves as a secondary element. On the other hand, if some physical mechanism is able to carry the C and O nuclei produced in the He-burning zones out to the H-burning zones, then the synthesized nitrogen behaves like a primary element.

3.3 Nitrogen yields in LIMS

Low- and intermediate-mass (LIM) stars, during the AGB phase, eject into the ISM significant amounts of He, C and N. The ejected masses reflect important abundance variations. The main physical mechanism for the transport of the C and O nuclei to the outer zones of the star is given by the so-called third dredge-up, which is the transfer of the nucleosynthetic products of the triple-α process by the surface convection which proceeds after each thermal pulse. Primary nitrogen can then be produced when the hot-bottom burning (CNO burning at the base of the convective envelope) occurs in combination with the third dredge-up (see, for example, Ventura et al. 2013).

In Fig. 2, we show how the stellar yields of Ventura et al. (2013) for C, O, and primary and secondary N vary as a function of the initial stellar mass, for different metalliticities. The stellar yield of a given chemical element X is defined as the ejected amount of mass of the newly formed X. By looking at the figure, the stellar

yields of secondary N increase with metallicity, by means of the consumption of the C and O nuclei originally present in the star. In fact, during the CNO cycle, the global abundance of the CNO nuclei remains constant, while the relative abundances of each CNO element can significantly vary. By looking at Fig. 2, the stellar producers of primary N have masses in the range between ∼3 and 6 $M_\odot$. Furthermore, the production of primary N does not show any correlation with the consumption of the original C and O in the star, as expected.

3.4 Nitrogen yields in massive stars

In order to reproduce the observed plateau in the (N/O) ratio for the MW halo stars, Matteucci (1986) proposed that massive stars should produce only primary N at all metallicities, at variance with standard nucleosynthesis models predicting only secondary N from massive stars. This plateau was also later observed in damped Ly α (DLA) systems (Pettini et al. 2002, 2008) and blue, low metallicity star-forming dwarf galaxies (Thuan et al. 1995; Berg et al. 2012; Izotov et al. 2012; James et al. 2015, see Fig. 1), thus confirming that there should be primary N production in massive stars.

Maeder & Meynet (2000) and Meynet & Maeder (2002a) found that primary N can be produced in rapidly rotating massive stars, but only at very low metallicity. Their proposed main physical mechanism is given by the so-called rotational mixing, particularly efficient at very low metallicity, where stars are expected to rotate faster and to be much more compact than their metal-rich counterparts. Rotational mixing allows the nucleosynthetic products of the triple-α reaction (mainly C and O nuclei) to efficiently diffuse towards the outer CNO burning zone, where a pure primary nitrogen can then be synthesized (Chiappini et al. 2008; Maeder 2009).

This unfortunately cannot solve the problem of the observed (N/O) plateau, which extends all over the metallicity range of MW halo stars. In fact, Geneva stellar evolutionary models predict fast rotating massive stars to produce primary N only in a narrow range at very low metallicity; as the metallicity $Z > 10^{-8}$, these stars resume producing only secondary N. Therefore, by assuming the theoretical stellar yields of the Geneva group, chemical evolution models predicted a 'dip' in the (N/O) ratio at low (O/H) abundances, which is never observed (see, for example, Chiappini et al. 2005, and the further discussion in Sections 3.5 and 6). To solve this discrepancy and be able to explain the observed trends in the data, all previous chemical evolution models (Matteucci 1986; Chiappini et al. 2005) had to assume artificially a pure primary N yield from massive stars.

3.5 Empirically fixing the nitrogen yield from massive stars at low metallicity

In order to re-assess the problem of primary nitrogen production in massive stars, we suggest a revised primary N stellar yield at low metallicity.

In Table 1, we report the IMF-averaged stellar yields of N and O from massive stars, $\overline{M}_{\rm N,R10}$ and $\overline{M}_{\rm O,R10}$, respectively, as computed by using the Romano et al. (2010) compilation of stellar yields and assuming the Kroupa et al. (1993) IMF. We also report how the values of log (N/O) are predicted to vary for different metallicities, when considering only the contributions of massive stars to the nitrogen and oxygen chemical enrichment of the ISM. We observe that the Geneva stellar models predict a dip in the (N/O) ratios for $Z > 10^{-8}$. This dip is never observed and it stems from the lack of primary N production by massive stars for $Z > 10^{-8}$.

Table 1. In this table, the various columns report the following quantities: (i) Z, metallicity; (ii) $\overline{M}_{\rm O,R10}$, the IMF-averaged stellar yield of oxygen in the mass range M = 11–100 $M_\odot$, by assuming the stellar yields of Romano et al. (2010, R10) and the Kroupa, Tout & Gilmore (1993) IMF; (iii) $\overline{M}_{\rm N,R10}$, the IMF-averaged stellar yield of nitrogen, defined as in the previous column; (iv) predicted average log (N/O) ratios, when considering only the contributions of massive stars; (v) average stellar yield of primary N which should be provided by massive stars to reproduce the observed low-metallicity plateau with log (N/O) ≈ −1.6 dex. This empirically derived yield is used as the reference stellar yield for primary nitrogen at low metallicity in this work.

Z	$\overline{M}_{\rm O,R10}$ ($M_\odot$)	$\overline{M}_{\rm N,R10}$ ($M_\odot$)	log (N/O)$_{\rm R10}$	$\overline{M}_{\rm N,prim}$ ($M_\odot$)
1.0×10^{-10}	3.025	0.014	−2.27	0.066
1.0×10^{-8}	3.105	0.082	−1.52	0.068
1.0×10^{-5}	1.995	0.0005	−3.53	0.043
1.0×10^{-3}	1.999	0.005	−2.55	0.044
4.0×10^{-3}	2.013	0.018	−1.99	0.044

In order to reproduce the low-metallicity plateau, we therefore calculate the average amount of primary N that massive stars should provide to reproduce the observed (N/O) plateau at very low metallicities. We assume that the oxygen yields in this regime are reliable and we require the predicted (N/O) ratios to match the observed log (N/O) ≈ −1.6 dex at low metallicity. In particular, we empirically derive the needed average stellar yield of primary nitrogen by massive stars as

$$\overline{M}_{\rm N,prim}(Z) = \overline{M}_{\rm O,R10}(Z) \times 10^{-1.6} \times \frac{A_{\rm N}}{A_{\rm O}}, \quad (1)$$

where $A_{\rm N}$ and $A_{\rm O}$ represent the atomic weight of N and O, respectively. The calculated values of $\overline{M}_{\rm N,prim}(Z)$ are reported in the last column of Table 1. Interestingly, at extremely low Z, the latter are of the same order of magnitude as the value of 0.065 $M_\odot$ originally adopted in chemical evolution models to reproduce the low-metallicity plateau (see also Chiappini et al. 2005, and references therein).

For the rest of this work, in our reference chemical evolution models, we assume a pure primary N production by massive stars, with the stellar yields at the various metallicities being the quantity $\overline{M}_{\rm N,prim}(Z)$, as given in equation (1) and reported in the last column of Table 1. We remark on the fact that, because of the way we have defined it, this quantity depends on the assumed IMF and stellar yields of oxygen.

4 THE CHEMICAL EVOLUTION FRAMEWORK

In this work, we study the nitrogen and oxygen evolution in the ISM of galaxies by adopting a chemical evolution model in which the galaxy is assumed to be composed of a single zone within which the various chemical elements are assumed to mix instantaneously and uniformly. The basic ingredients of the model are described in detail in Matteucci (2012). In summary, the model is capable of following the temporal evolution of the abundances of various chemical elements within the ISM of galaxies, by taking into account the main physical processes driving chemical evolution, such as star formation, inflows and outflows of gas.

4.1 Star formation and chemical evolution

By defining $M_{{\rm g},i}(t)$ as the gas mass in the galaxy which is in the form of the ith chemical element at time t, its temporal evolution

follows:

$$\frac{\mathrm{d}M_{\mathrm{g},i}(t)}{\mathrm{d}t} = \underbrace{-X_i(t)\,\mathrm{SFR}(t)}_{\mathrm{SF}} + \underbrace{R_i(t)}_{\mathrm{yields}} - \underbrace{\Psi_i(t)}_{\mathrm{outflow}} + \underbrace{\Phi_i(t)}_{\mathrm{infall}}, \quad (2)$$

where $X_i(t) = M_{\mathrm{g},i}(t)/M_{\mathrm{g}}(t)$ is the abundance by mass of the ith chemical element, defined such that $\sum_i X_i(t) = 1$, and $M_{\mathrm{g}}(t)$ is the total gas mass in the galaxy at time t. In our models, we assume the stellar lifetimes of Padovani & Matteucci (1993).

We assume a star formation law of the form $\mathrm{SFR}(t) = \nu M_{\mathrm{g}}(t)$, with ν being the star formation efficiency (SFE), a free parameter of our models.

The term $R_i(t)$ in equation (2) represents the rate at which stars return the ith chemical element back to the ISM at their death. This term subsumes all our prescriptions about the stellar yields as well as the assumptions concerning SN progenitors. In particular, for Type Ia SNe, we assume the 'single degenerate scenario' with the same prescriptions as in Matteucci & Recchi (2001) and Matteucci (2001, 2012), however, the details of the treatment of Type Ia SNe are largely irrelevant to this work, since they only have a very minor effect in the enrichment of oxygen and nitrogen.

4.2 The infall rate

In our model, the galaxy is assumed to assemble by means of accretion of gas from an external reservoir into the potential well of an underlying dark matter halo.

The gas infall rate, $\Phi_i(t)$, follows an exponential form with time given by

$$\Phi_i(t) = \frac{X_{\mathrm{inf},i}\, M_{\mathrm{inf}}\, e^{-t/\tau_{\mathrm{inf}}}}{\tau_{\mathrm{inf}}\left(1 - e^{-t_{\mathrm{G}}/\tau_{\mathrm{inf}}}\right)}, \ \text{with} \sum_i \int_0^{t_{\mathrm{G}}} \Phi_i(t)\mathrm{d}t = M_{\mathrm{inf}}, \quad (3)$$

where t_{G} is the age of the galaxy and $X_{\mathrm{inf},i}$ is the abundance by mass of the ith chemical element in the infalling gas (M_{inf}), whose chemical composition is assumed to be primordial.

4.3 The outflow model

In equation (2), the outflow rate is modelled by $\Psi_i(t) = \omega_i\,\mathrm{SFR}(t)$, where ω_i is the so-called mass loading factor. Observations generally suggest that star-forming galaxies experience time-averaged outflow loading factors of order unity (Lilly et al. 2013; Belfiore et al. 2015; Lu, Blanc & Benson 2015; Peng, Maiolino & Cochrane 2015) at stellar masses around $\log(M_\star/M_\odot) \sim 10$, close to the knee of the luminosity function. It is, however, likely that less massive galaxies experience much higher loading factors.

In this work, we assume the galactic wind to be differential; namely, the outflow carries only the main nucleosynthetic products of core-collapse SNe (mainly α-elements), for which ω_i is a constant value. For chemical elements such as nitrogen and carbon, which have a very minor contribution from SNe, we assume a null mass loading factor, i.e. $\omega_i = 0$. The assumption of a differential outflow is justified by the fact that massive stars (the progenitors of core-collapse SNe and the most important oxygen producers in the Universe) are observed to be highly clustered and so, as they explode, they create a region of the ISM in which the filling factor closely approaches to unity (see Marconi, Matteucci & Tosi 1994; Recchi, Matteucci & D'Ercole 2001).

Interestingly, the first works suggesting a differential metal-enhanced galactic wind in the context of the study of chemical evolution of galaxies were those of Pilyugin (1993) and Marconi et al. (1994), which addressed also the issue of explaining the (N/O) versus (O/H) abundance pattern observed in dwarf irregular galaxies (see Recchi et al. 2008 for a detailed study and references). We are aware that our assumption of a differential galactic wind is highly uncertain and it does not rely on firm theoretical and observational findings; further detailed investigations are needed, by looking – for example – at the chemical abundances in the halo of the MW or in quasar absorption lines, which were also related in the past to galactic winds.

Following the formalism of Bradamante, Matteucci & D'Ercole (1998), the time for the onset of the galactic outflow is calculated by requiring the thermal energy of the gas (supplied by SNe and stellar winds to the galaxy ISM) to be larger than the binding energy of the gas to the galaxy potential well.

4.4 Summary of the stellar yields for O and N

In this work, we assume for oxygen and nitrogen the following set of stellar yields.

(i) For massive stars, we assume the metallicity-dependent compilation of stellar yields of Romano et al. (2010), in which the nitrogen and oxygen yields have been computed by the Geneva group, by including the combined effect of rotation and mass loss (see, for more details, Meynet & Maeder 2002b; Hirschi, Meynet & Maeder 2005; Hirschi 2007; Ekström et al. 2008). For $Z < 10^{-3}$, we make use of the empirically motivated nitrogen yield of massive stars derived in Section 3.5.

(ii) For LIM stars, we assume the stellar yields at the various metallicities computed by means of the ATON numerical code of stellar evolution (see, for a detailed description, Mazzitelli 1989; Ventura et al. 1998; Ventura & D'Antona 2009; Ventura et al. 2013). We have chosen the Ventura et al. (2013) stellar yields because they provide separately the primary and secondary components of the nitrogen stellar yield for a large range of metallicities ($3.0 \times 10^{-4} \leq Z \leq 0.04$; see the discussion in Section 3.1). Other works which also separate the two components are those of Gavilán, Buell & Mollá (2005) and Gavilán et al. (2006), however, they span a too narrow metallicity range for the purpose of our work.

5 MODELLING THE SDSS DATA

In this section, we compare the predictions of our chemical evolution models with the set of data discussed in Section 2 (see Fig. 1) focusing on reproducing the high-metallicity regime of the (N/O) versus (O/H) diagram. We will address the question of reproducing the low-metallicity tail of the (N/O) distribution in the next section.

5.1 The reference model

Given the relatively large number of free parameters in our detailed chemical evolution model, we take a qualitative, staged approach. We first choose a set of reference parameters. We then investigate the effect of changing each of them, while keeping the other ones fixed. Our reference model assumes:

(i) fixed SFE $\nu = 1.5\,\mathrm{Gyr}^{-1}$,
(ii) fixed mass loading factor $\omega = 0.8$ for oxygen,
(iii) differential galactic outflow, with $\omega = 0.0$ for nitrogen,
(iv) infall mass $\log(M_{\mathrm{inf}}/\mathrm{M}_\odot) = 10.25$,
(v) infall time-scale $\tau_{\mathrm{inf}} = 1\,\mathrm{Gyr}$,
(vi) Kroupa et al. (1993) IMF,

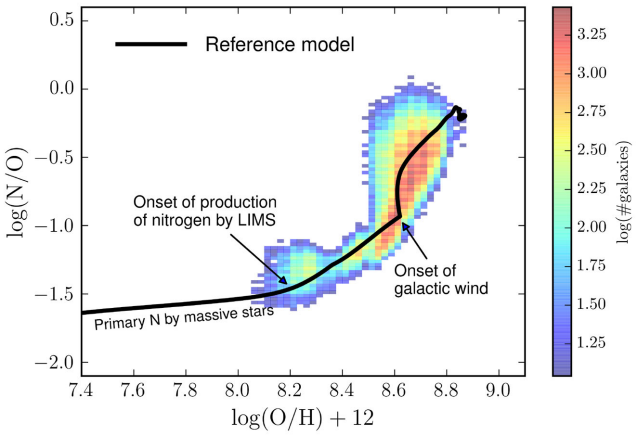

Figure 3. The reference chemical evolution model used in this work to reproduce the abundance pattern in the (N/O) versus (O/H) plane (black solid line). The distribution of SDSS galaxies is shown as a 2D histogram, with the bin size in both the (N/O) and (O/H) dimensions being 0.025 dex, and the colour-coding represents the number of galaxies in each bin. The changes in slope of the observed (N/O) versus (O/H) relation are linked to different physical properties of the model. The plateau at low metallicity is due to the pure primary N production by massive stars. The slope of the (N/O) versus (O/H) relation increases when LIMS start dying, producing both primary and secondary nitrogen. A further steepening of the relation is obtained after the onset of a differential galactic wind, which here is assumed to expel oxygen preferentially.

and the star formation history is assumed to be extended over all the galaxy lifetime (i.e. we do not introduce a quenching phase). In Fig. 3, we plot this reference model in the (N/O) versus (O/H) plane, together with the distribution of SDSS galaxies. The observed (N/O) versus (O/H) abundance pattern is shown as a density plot, with the bin size in both the (N/O) and (O/H) dimensions being 0.025 dex; we show only the bins which contain more than 10 galaxies and the colour-coding represents the number of galaxies within each bin.

It is remarkable to note that our simple reference model in Fig. 3 can well reproduce the main features of the data. The predicted low-metallicity plateau is the effect of our assumption of a pure primary N production by massive stars. The increase of the (N/O) ratios from $12 + \log(\mathrm{O/H}) \sim 8.0$ dex is due to the delayed chemical feedback of LIMS, which pollute the ISM with primary and secondary nitrogen; we will refer to this change in slope as the 'first break point'. By definition, the production of secondary nitrogen by LIMS increases as the metallicity increases. Although the production of primary N is smaller than the one of secondary N (see Fig. 2), the main primary N producers turns out to be, on average, less massive and hence more long-living than the bulk of the secondary N producers. In this way, the pollution of the ISM with primary N by LIMS mimics and amplifies the secondary N component. At $12 + \log(\mathrm{O/H}) \sim 8.6$ dex, we see in Fig. 3 a new change in slope ('second break point'), which is caused by the onset of the galactic wind. Since we assume a differential outflow, the loss of oxygen per unit time is more efficient than the loss of nitrogen (which is set to zero). In this way, the accumulation of oxygen within the galaxy ISM slows down and the net effect of the galactic wind is to steepen the (N/O) ratios as the chemical evolution proceeds. We remark that the increase of the (N/O) ratios after the second break point is also crucially bolstered by the larger amounts of secondary N which LIMS are able to synthesize at higher Z.

5.2 Exploring the parameter space

In this section, we discuss the effect of varying the free parameters in the reference model. In particular, we show that the main parameters influencing the shape of the (N/O) versus (O/H) relation are the SFE, the outflow loading factor and the assumptions regarding the differential outflow loading for N and O. Other parameters, such as the infall mass and the infall time-scale do not have a significant effect on the abundance trends studied.

5.2.1 The infall mass

In Fig. 4(a), we explore the effect of varying the infall mass, in the range $\log(M_{\rm inf}/\mathrm{M}_{\odot}) = 9.75$–$11.0$. The common evolution of all the galaxies before the onset of the galactic wind stems from the fact that all these models assume a fixed SFE ($\nu = 1.5\,\mathrm{Gyr}^{-1}$). The models developing the galactic wind first are the ones with the smallest infall mass, which depart from the common track at the lowest (O/H) abundances; in fact, such models are characterized by a lower galaxy potential well, and hence they develop the outflow at earlier times. Overall the infall mass in our models does not play a key role in defining the shape of the (N/O) versus (O/H) relation.

5.2.2 The infall time-scale

The infall time-scale regulates the rate of accretion of the gas into the system. In particular, by fixing the values of the other parameters, models with longer infall time-scales predict the galactic wind to develop at earlier times, since the binding energy of the gas to the whole galaxy is lower, at any time of the galaxy evolution. This can be appreciated by looking at Fig. 4(b), where models assuming different infall time-scales are compared. Before the onset of the galactic wind, all the models evolve on the same track in the (N/O) versus (O/H) diagram because the SFE is kept fixed.

5.2.3 The SFE

The SFE (ν) is a key parameter in driving the star formation history of the system and has a complex effect on the balance of the different stellar populations that contribute to the nitrogen and oxygen abundance in galaxies. Increasing the SFE speeds up the production of oxygen per unit time by massive stars in the earliest stages of the galaxy chemical evolution. Since we assume that nitrogen is synthesized by massive stars as a pure primary element, the increasing of the SFE does not affect much the (N/O) ratio in the low-metallicity regime.

In Fig. 4(c), we explore the effect of varying the SFE in the range $\nu = 0.5$–$3\,\mathrm{Gyr}^{-1}$. The first large effect in the (N/O) versus (O/H) diagram can be seen at the first break point; in particular, the higher the SFE, the larger is the metal content within the galaxy as first LIMS die, causing the (N/O) ratios to increase. In conclusion, an increase of the SFE determines a wider range in metallicity of the initial (N/O) plateau due to the chemical enrichment of massive stars. This is a sort of application of the so-called time-delay model (Tinsley 1979; Greggio & Renzini 1983; Matteucci & Greggio 1986) to the (N/O) versus (O/H) diagram. We remind the reader that by time-delay model, we mean the classical way of interpreting the trend of the observed [α/Fe] versus [Fe/H] abundance patterns in galaxies, where key roles are played by the assumed SFE and the delayed chemical enrichment by Type Ia SNe; in particular, the higher the SFE in galaxies, the larger is the [Fe/H] abundance

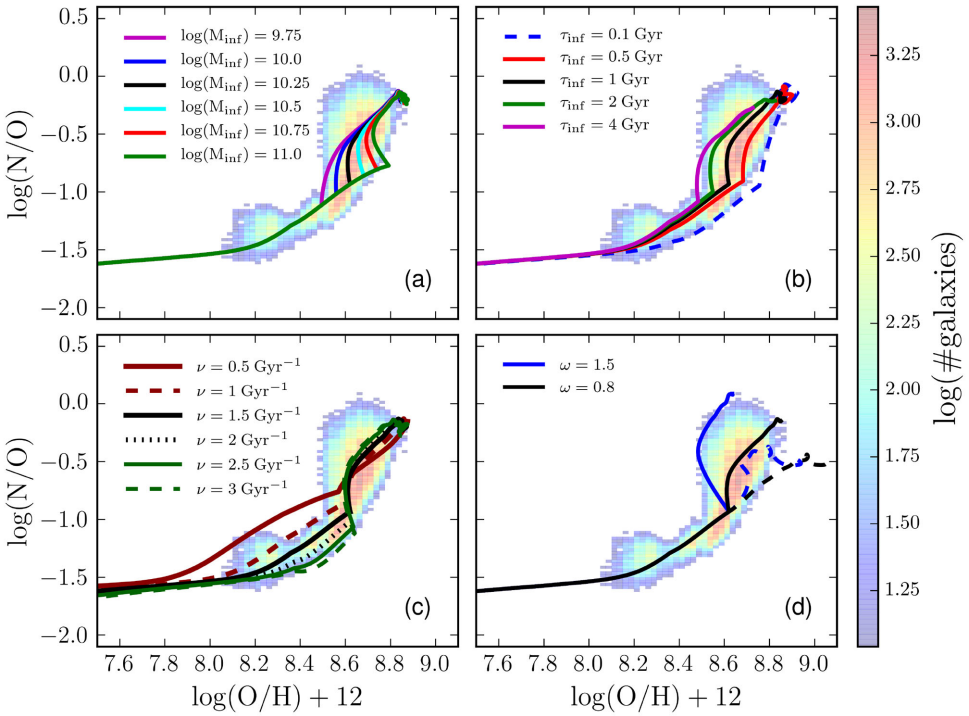

Figure 4. Chemical evolution model track in the (N/O) versus (O/H) plane. Abundances for SDSS galaxies are shown as a 2D histogram, with the colour-coding corresponding to the number of galaxies in each bin, with the bin size in both the (N/O) and (O/H) dimensions being 0.025 dex. The reference model is always plotted in black solid line. In different panels, we vary different free parameters of the chemical evolution model. In panel (a), we change the infall mass $M_{\rm inf}$; in panel (b), the infall time-scale $\tau_{\rm inf}$; in panel (c), the SFE ν; and in panel (d), the outflow loading factor ω. In panel (d), the dashed lines correspond to a non-differential outflow (where both N and O are expelled with the same efficiency) while the solid lines refer to the reference assumption of a differential outflow where N is not expelled (with $\omega_{\rm N} = 0$).

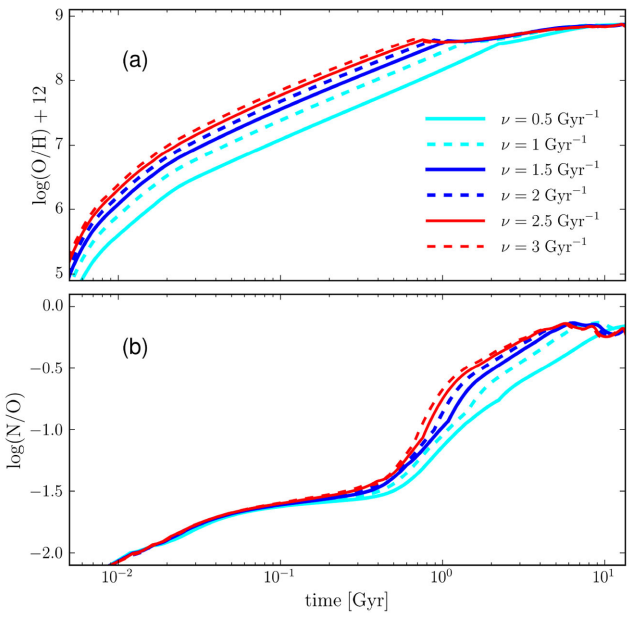

Figure 5. In this figure, in panels (a) and (b), we show how the (O/H) abundances and the (N/O) ratios, respectively, are predicted to vary as functions of the galaxy time. The various curves correspond to models with different star formation efficiency, with the reference model being the blue solid line.

of the ISM as first Type Ia SNe explode and hence the [α/Fe] ratios steeply decrease.

In Fig. 5(a), we show the relations between the age of the galaxy and the metallicity of the ISM, as predicted by our models with varying star formation efficiencies (SFEs). Galaxies with very low SFEs struggle to reach high (O/H) abundances, spending most of their evolutionary time at low metallicities. Conversely, models with higher SFEs predict galaxies to reach the (O/H) abundances of the SDSS data at earlier times. Once the galactic wind develops, there is an interplay between the rate of restitution of oxygen into the galaxy ISM by dying stars and the rate of removal of oxygen by galactic wind and star formation; this causes the (O/H) abundances to increase more gradually with time than before the onset of the galactic wind.

In Fig. 5(b), we show how the predicted (N/O) ratios vary as a function of the time, when varying the SFE. In the earliest stages of the galaxy evolution, all the models tend towards $\log({\rm N/O}) \sim -1.6$ dex, which corresponds to the nitrogen-to-oxygen ratio of the low-metallicity plateau. As first LIMS die, the (N/O) ratio is predicted to suddenly increase, because of the large amounts of both primary and secondary N which LIMS are capable of synthesize. In summary, the higher the SFE, the earlier and the higher are the metallicities (as discussed above) when LIMS start dying, causing the (N/O) ratio to increase. The effect of the onset of the galactic wind is less visible in this figure, and it corresponds to the gradual change in the slope of the (N/O) versus time relation occurring at later times.

5.2.4 The outflow loading factor

Our reference model assumes a differential outflow, which carries only the nucleosynthetic products of core-collapse SNe (mainly α-elements) out of the galaxy potential well. Hence the mass loading factor, ω, quoted in the reference model only refers to oxygen,

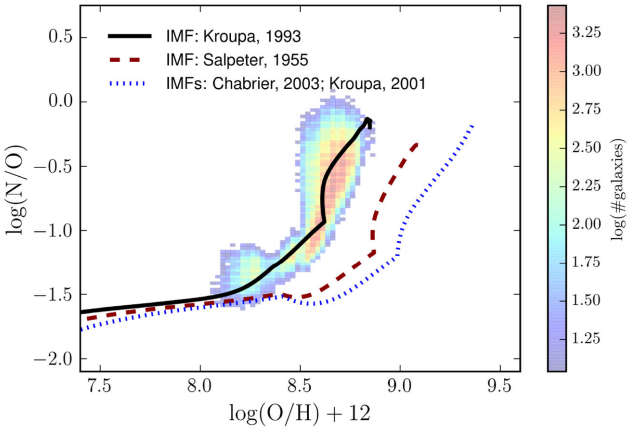

Figure 6. In this figure, we explore the effect of changing the IMF on the predicted (N/O) versus (O/H) diagram. The black solid curve corresponds to our reference model with the Kroupa et al. (1993) IMF, the dashed curve in dark red to the Salpeter (1955) IMF, and the dotted curve in blue to the Chabrier (2003) and Kroupa (2001) IMFs, which provide very similar final results.

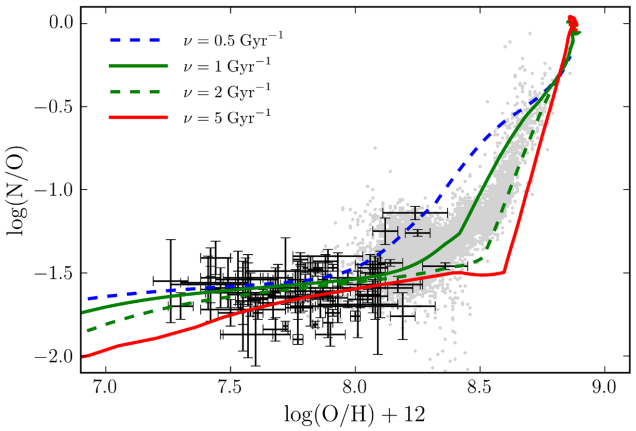

Figure 7. In this figure, we show chemical evolution models for dwarf galaxies. We assume $M_{\rm inf} = 10^9$ M$_\odot$, varying SFEs, an infall time-scale $\tau_{\rm inf} = 0.1$ Gyr and the IMF of Kroupa et al. (1993). The grey points correspond to the SDSS galaxies with $M_\star \leq 10^9\,M_\odot$, in the same range of stellar mass as the metal-poor, star-forming dwarf galaxies from Berg et al. (2012), Izotov et al. (2012) and James et al. (2015), which are represented by the data with error bars.

since nitrogen is assumed not to be expelled. Obviously, in reality, some nitrogen would be lost to the IGM, but here we consider its mass loading factor to be much lower than the one of oxygen, since core-collapse SNe are minor contributors of N in galaxies and the galactic wind (mainly triggered by SN explosions) develops when LIMS have already heavily polluted the ISM with nitrogen, overcoming the N enrichment from massive stars.

In Fig. 4(d), we show the effect of almost doubling the mass loading factor on the (N/O) versus (O/H) abundance pattern. By definition, this parameter only has an effect after the galactic wind has started; this occurs at $12 + \log$ (O/H) ~ 8.6 dex in our reference model. The requirement of a differential outflow to reproduce the observed trend of the (N/O) versus (O/H) abundance pattern can be appreciated by comparing the solid and dashed curves in Fig. 4(d), corresponding to models with differential and non-differential outflow, respectively. Concerning the model with a differential outflow, ω has the clear effect of changing the slope of the (N/O) versus (O/H) relation at high metallicity. Importantly, even in the case of the reference model, this slope is much steeper than unity, which is the naive prediction for the secondary nitrogen enrichment. By looking at equation (2), the slope is crucially determined by the balance between the loss of oxygen via galactic winds (and star formation) and the restitution of oxygen by massive stars. If the latter exceeds the former, the slope is positive, otherwise it is negative. Concerning the model with a non-differential outflow, the transition between the SF-dominated regime and the outflow-dominated regime is smooth, since both oxygen and nitrogen are lost from the galaxy potential well with the same efficiency ω.

5.2.5 The IMF

In Fig. 6, we explore the effect of changing the IMF on the (N/O) versus (O/H) abundance diagram. Our reference IMF, which is Kroupa et al. (1993, the best IMF for the MW disc; see Romano et al. 2010), hosts a large number of LIMS and a much smaller number of massive stars than the Salpeter (1955) IMF, and it provides the best agreement with the observed data set among the classical initial mass functions (IMFs) considered in this work. IMFs like Chabrier (2003) and Kroupa (2001), which are very similar among each other, host a larger number of massive stars and hence an enhanced oxygen-production is predicted at the early stages of galaxy evolution; so the first break point occurs at higher metallicities when the Chabrier (2003) or the Kroupa (2001) IMF are assumed. The main effect of the IMF is to shift the chemical evolution tracks along the (O/H) axis. In fact, the main role of the IMF is to assign different weights to stars in different mass ranges.

6 MODELLING THE LOW-METALLICITY TAIL

In this subsection, we present chemical evolution models for star forming, metal-poor dwarf galaxies, in order to reproduce the observed low-metallicity tail of the (N/O) ratios. The data of Berg et al. (2012), Izotov et al. (2012) and James et al. (2015) clearly exhibit a plateau in the (N/O) ratios, which extends towards low (O/H) abundances. None of the models developed in the past has been capable of reproducing this trend (see Chiappini et al. 2005).

In Fig. 7, we show the predictions of models with $M_{\rm inf} = 10^9$ M$_\odot$, $\tau_{\rm inf} = 0.1$ Gyr and SFEs in the range $\nu = 0.05$–5 Gyr^{-1}, with the purpose of reproducing the trend of the (N/O) versus (O/H) abundances which are observed in metal-poor star-forming dwarf galaxies (data with error bars) and in the SDSS galaxies with stellar mass $M_\star \leq 10^9$ M$_\odot$. The other parameters are the reference ones, as described at the beginning of Section 5. In these models, we assume that massive stars produce pure primary N; our stellar yields for N are summarized in Table 1, and they have been computed as a function of the metallicity, starting from the observational constraint that metal-poor dwarf galaxies share a common nitrogen-to-oxygen ratio which is log (N/O) ≈ -1.6 dex.

The trend of the various models in Fig. 7 can be explained by means of the same mechanism which has been mentioned throughout all the text: very low SFEs cause a slow production of oxygen by massive stars; this fact allows the ISM to be quite metal-poor when LIMS begin to highly pollute the ISM with nitrogen. Therefore, lowering the SFEs causes the plateau of the (N/O) ratios to be less extended in metallicity and hence the first break to occur at lower Z. This explanation is a sort of application of the time-delay model to the (N/O) versus (O/H) diagram. By comparing models and data,

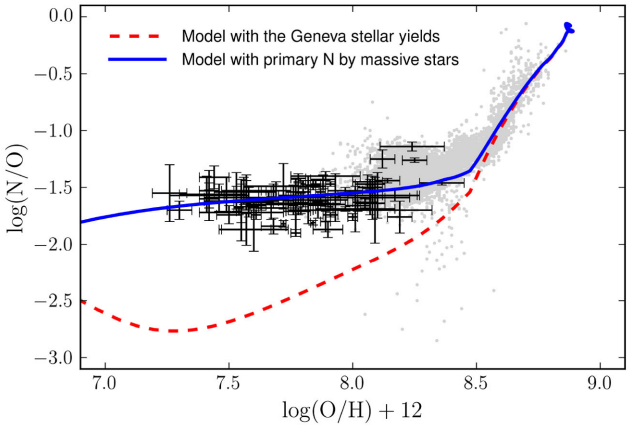

Figure 8. In this figure, we compare the predictions of a model with pure primary N production by massive stars with a similar model assuming the Geneva stellar yields for massive stars, as given in Romano et al. (2010, their model 15). Both models assume $\nu = 1.5\,\mathrm{Gyr}^{-1}$, $M_{\rm inf} = 10^9\,\mathrm{M}_\odot$ and $\tau_{\rm inf} = 0.1\,\mathrm{Gyr}$. The data are same as in Fig. 7.

we can obtain a good qualitative agreement, clearly suggesting that a pure primary N production by massive stars is needed to explain and reproduce the low-metallicity plateau.

By assuming the N stellar yields of massive stars collected by Romano et al. (2010), which include the results of the stellar evolutionary code of the Geneva group taking into account the effects of mass loss and rotation, all our chemical evolution models predict a dip in the (N/O) ratios when going towards low (O/H) abundances (see also Table 1), at variance with observations.

This can be appreciated by looking at Fig. 8, where the predictions of a model with pure primary N production by massive stars is compared with a similar model assuming the Geneva stellar yields for massive stars, as given in Romano et al. (2010, their model 15). Both models assume $\nu = 1.5\,\mathrm{Gyr}^{-1}$, $M_{\rm inf} = 10^9\,\mathrm{M}_\odot$ and $\tau_{\rm inf} = 0.1\,\mathrm{Gyr}$. Fig. 8 clearly points out the still open problem of standard stellar nucleosynthesis calculations as well as of stellar evolutionary models to predict the right amount of pure primary N which massive stars should provide to reproduce the observed (N/O) plateau at very low metallicity.

7 CONCLUSIONS

In this article, we have presented a set of chemical evolution models with the purpose of reproducing the (N/O) versus (O/H) abundance pattern, as observed in a sample of SDSS galaxies (Abazajian et al. 2009) and metal-poor, star-forming dwarf galaxies (Berg et al. 2012; Izotov et al. 2012; James et al. 2015). Our collection of data spans a wide metallicity range ($7.1\,\mathrm{dex} \lesssim \log(\mathrm{O/H}) + 12 \lesssim 8.9\,\mathrm{dex}$), enabling us to recover the trend of the observed (N/O) versus (O/H) relation with a precision never reached before. At very low metallicity, the data clearly demonstrate the existence of a plateau in the (N/O) ratio, followed by an increase of this ratio which steepens as the metallicity increases. We summarize our main conclusions in what follows.

(i) The low-metallicity plateau in the nitrogen-to-oxygen ratio represents the imprint of pure primary N from massive stars, as originally suggested by Matteucci (1986). Such plateau is also observed all over the metallicity range of MW halo stars and in low-metallicity DLAs. From a theoretical point of view, standard nucleosynthesis calculations have shown that the rotational mixing in very-metal poor massive stars can allow a pure primary N production (see Maeder & Meynet 2000, and subsequent papers from the Geneva group); nevertheless, as the metallicity becomes $Z > 10^{-8}$, massive stars resume producing only secondary N. This still represents an open problem in stellar nucleosynthesis calculations, since all the chemical evolution models with the current stellar yields of massive stars, including standard mass loss and rotation, predict a 'dip' in the (N/O) ratios for $Z > 10^{-8}$, at variance with observations (see, for example, Chiappini et al. 2005; Romano et al. 2010).

(ii) In this work, we have computed the primary N stellar yields of massive stars which are needed, as functions of the metallicity, to reproduce the observational constraint suggesting that $\log(\mathrm{N/O}) \approx -1.6\,\mathrm{dex}$ in metal-poor, star-forming dwarf galaxies. Our results are given in the last column of Table 1. In this way, we have been able to reproduce the observed flat trend of the data.

(iii) A fundamental aspect to take into account for explaining the trend of the observed (N/O) versus (O/H) abundance pattern is the time-delay with which LIMS start enriching the ISM with both primary and secondary N. In fact, before the first LIMS die, massive stars are the only nitrogen and oxygen producers in galaxies. When LIMS start dying, the N abundance within the galaxy ISM steeply increases. Since the stellar yields of the secondary N component by LIMS increase with metallicity, then the (N/O) ratios continuously grow as a function of the (O/H) abundance.

(iv) The range in metallicity of the initial (N/O) plateau in the (N/O) versus (O/H) abundance diagram is determined by the SFE; in particular, the higher the SFE, the larger is the extension in metallicity of the plateau. In fact, the SFE is the main parameter driving the rate of metal production from massive stars, hence regulating the metallicity of the system when LIMS begin to heavily pollute the ISM with nitrogen. Therefore, if the SFE is high, the change in slope of the (N/O) ratio occurs at higher metallicity than in the case with low SFE. This is a consequence of the so-called time-delay model on the (N/O) versus (O/H) diagram. In conclusion, the position of the galaxies along the observed (N/O) versus (O/H) sequence is mostly determined by the SFE.

(v) Only by assuming differential galactic winds, removing exclusively chemical elements produced in core-collapse SNe, we have been able to reproduce the steep increasing trend of (N/O) ratios at high metallicity. Nevertheless, the larger amounts of secondary N provided by LIMS as the metallicity increases is necessary to reach the high observed (N/O) ratios at high metallicity. In our reference model, we have assumed a mass loading factor of the order of the unity; the variation of this parameter crucially determines the slope with which the (N/O) ratios are observed to increase at high metallicity. On the other hand, all our models with normal galactic wind – in which all the chemical elements are carried out of the galaxy potential well with the same efficiency – fail in explaining the observed trend of the (N/O) versus (O/H) abundance pattern.

(vi) The role of the IMF consists in giving different weights to stars as functions of their mass, when the star formation process takes place. If the IMF is rich in massive stars, then an enhanced O production is predicted (see also Vincenzo et al. 2016), letting the (N/O) ratios start to increase at high (O/H) abundances. So the main effect of the IMF is to shift the (N/O) versus (O/H) relations over the (O/H) axis. Our chemical evolution models with the Kroupa et al. (1993) IMF provide the best agreement with the observed data set.

ACKNOWLEDGEMENTS

FV thanks the Cavendish Astrophysics Group at the University of Cambridge for kindly supporting his visit during 2014 September.

FB acknowledges funding from the United Kingdom Science and Technology Facilities Council (STFC). RM acknowledges funding from the United Kingdom STFC through grant ST/M001172/1. FM acknowledges financial support from PRIN-MIUR 2010-2011 project 'The Chemical and Dynamical Evolution of the Milky Way and Local Group Galaxies', prot. 2010LY5N2T. We thank an anonymous referee for his/her constructive comments, which have improved the clarity of the paper. The data used in this paper can be retrieved at the MPA-JHU DR7 release of spectrum measurements web page: http://wwwmpa.mpa-garching.mpg.de/SDSS/DR7/.

REFERENCES

Abazajian K. N. et al., 2009, ApJ, 182, 543
Aihara H. et al., 2011, ApJ, 193, 29
Alloin D., Collin-Souffrin S., Joly M., Vigroux L., 1979, A&A, 78, 200
Andrews B. H., Martini P., 2013, ApJ, 765, 140
Baldwin J. A., Phillips M. M., Terlevich R., 1981, PASP, 93, 5
Belfiore F. et al., 2015, MNRAS, 449, 867
Belfiore F., Maiolino R., Bothwell M., 2016, MNRAS, 455, 1218
Berg D. A. et al., 2012, ApJ, 754, 98
Bernardi M. et al., 2003, AJ, 125, 1882
Blanc G. A., Kewley L., Vogt F. P. A., Dopita M. A., 2015, ApJ, 798, 99
Bolatto A. D. et al., 2013, Nature, 499, 450
Bothwell M. S., Maiolino R., Kennicutt R., Cresci G., Mannucci F., Marconi A., Cicone C., 2013, MNRAS, 433, 1425
Bradamante F., Matteucci F., D'Ercole A., 1998, A&A, 337, 338
Brinchmann J., Charlot S., White S. D. M., Tremonti C., Kauffmann G., Heckman T., Brinkmann J., 2004, MNRAS, 351, 1151
Calura F., Pipino A., Matteucci F., 2008, A&A, 479, 669
Calzetti D., 2001, PASP, 113, 1449
Cardelli J. A., Clayton G. C., Mathis J. S., 1989, ApJ, 345, 245
Caselli P., Walmsley C. M., Zucconi A., Tafalla M., Dore L., Myers P. C., 2002, ApJ, 565, 344
Chabrier G., 2003, PASP, 115, 763
Charlot S., Fall S. M., 2000, ApJ, 539, 718
Chiappini C., Romano D., Matteucci F., 2003, MNRAS, 339, 63
Chiappini C., Matteucci F., Ballero S. K., 2005, A&A, 437, 429
Chiappini C., Ekström S., Meynet G., Hirschi R., Maeder A., Charbonnel C., 2008, A&A, 479, L9
Cicone C. et al., 2014, A&A, 562, A21
Cicone C. et al., 2015, A&A, 574, A14
da Cunha E., Eminian C., Charlot S., Blaizot J., 2010, MNRAS, 403, 1894
Davé R., Finlator K., Oppenheimer B. D., 2012, MNRAS, 421, 98
Dekel A., Zolotov A., Tweed D., Cacciato M., Ceverino D., Primack J. R., 2013, MNRAS, 435, 999
Driver S. P. et al., 2011, MNRAS, 413, 971
Dwek E., 1998, ApJ, 501, 643
Dwek E., Cherchneff I., 2011, ApJ, 727, 63
Edmunds M. G., 2001, MNRAS, 328, 223
Edmunds M. G., Pagel B. E. J., 1978, MNRAS, 185, 77P
Ekström S., Meynet G., Chiappini C., Hirschi R., Maeder A., 2008, A&A, 489, 685
Erb D. K., 2008, ApJ, 674, 151
Erb D. K., 2015, Nature, 523, 169
Fabian A. C., 2012, ARA&A, 50, 455
Faucher-Giguère C.-A., Kereš D., Ma C.-P., 2011, MNRAS, 417, 2982
Feldmann R., 2015, MNRAS, 449, 3274
Finlator K., Davé R., 2008, MNRAS, 385, 2181
Fisher D. B. et al., 2014, Nature, 505, 186
Fraternali F., Binney J. J., 2008, MNRAS, 386, 935
Fraternali F., van Moorsel G., Sancisi R., Oosterloo T., 2002, AJ, 123, 3124
Fraternali F., Marasco A., Armillotta L., Marinacci F., 2015, MNRAS, 447, L70
Gavilán M., Buell J. F., Mollá M., 2005, A&A, 432, 861
Gavilán M., Mollá M., Buell J. F., 2006, A&A, 450, 509
Geach J. E. et al., 2014, Nature, 516, 68
Gentile G. et al., 2013, A&A, 554, A125
Greggio L., Renzini A., 1983, Mem. Soc. Astron. Ital., 54, 311
Heald G. et al., 2011, A&A, 526, A118
Henry R. B. C., Edmunds M. G., Köppen J., 2000, ApJ, 541, 660
Hirschi R., 2007, A&A, 461, 571
Hirschi R., Meynet G., Maeder A., 2005, A&A, 433, 1013
Hjorth J., Gall C., Michałowski M. J., 2014, ApJ, 782, L23
Hopkins P. F., Quataert E., Murray N., 2012, MNRAS, 421, 3522
Hughes T. M., Cortese L., Boselli A., Gavazzi G., Davies J. I., 2013, A&A, 550, A115
Izotov Y. I., Thuan T. X., Guseva N. G., 2012, A&A, 546, A122
James B. L., Koposov S., Stark D. P., Belokurov V., Pettini M., Olszewski E. W., 2015, MNRAS, 448, 2687
Jenkins E. B., 2009, ApJ, 700, 1299
Kauffmann G. et al., 2003, MNRAS, 341, 33
Kewley L. J., Ellison S. L., 2008, ApJ, 681, 1183
Kewley L. J., Dopita M. A., Sutherland R. S., Heisler C. A., Trevena J., 2001, ApJ, 556, 121
Köppen J., Hensler G., 2005, A&A, 434, 531
Kroupa P., 2001, MNRAS, 322, 231
Kroupa P., Tout C. A., Gilmore G., 1993, MNRAS, 262, 545
Lequeux J., Peimbert M., Rayo J. F., Serrano A., Torres-Peimbert S., 1979, A&A, 80, 155
Lilly S. J. et al., 2009, ApJS, 184, 218
Lilly S. J., Carollo C. M., Pipino A., Renzini A., Peng Y., 2013, ApJ, 772, 119
Lisenfeld U., Ferrara A., 1998, ApJ, 496, 145
López-Sánchez Á. R., Dopita M. A., Kewley L. J., Zahid H. J., Nicholls D. C., Scharwächter J., 2012, MNRAS, 426, 2630
Lu Y., Blanc G. A., Benson A., 2015, ApJ, 808, 129
Maeder A., 2009, Physics, Formation and Evolution of Rotating Stars, Astronomy and Astrophysics Library. Springer-Verlag, Berlin, Heidelberg, 2009
Maeder A., Meynet G., 2000, A&A, 361, 159
Mannucci F., Cresci G., Maiolino R., Marconi A., Gnerucci A., 2010, MNRAS, 408, 2115
Marconi G., Matteucci F., Tosi M., 1994, MNRAS, 270, 35
Matteucci F., 1986, MNRAS, 221, 911
Matteucci F., 1994, A&A, 288, 57
Matteucci F., 2001, Astrophysics and Space Science Library, Vol. 253, The Chemical Evolution of the Galaxy. Kluwer, Dordrecht
Matteucci F., 2012, Chemical Evolution of Galaxies, Astronomy and Astrophysics Library. Springer-Verlag, Berlin, Heidelberg
Matteucci F., Greggio L., 1986, A&A, 154, 279
Matteucci F., Recchi S., 2001, ApJ, 558, 351
Mazzitelli I., 1989, ApJ, 340, 249
Meyer D. M., Cardelli J. A., Sofia U. J., 1997, ApJ, 490, L103
Meynet G., Maeder A., 2002a, A&A, 381, L25
Meynet G., Maeder A., 2002b, A&A, 390, 561
Mollá M., Vílchez J. M., Gavilán M., Díaz A. I., 2006, MNRAS, 372, 1069
Oosterloo T., Fraternali F., Sancisi R., 2007, AJ, 134, 1019
Osterbrock D. E., Ferland G. J., 2006, Astrophysics of Gaseous Nebulae and Active Galactic Nuclei, 2nd edn. University Science Books, Mill Valley, CA
Padovani P., Matteucci F., 1993, ApJ, 416, 26
Pagel B. E. J., 2009, Nucleosynthesis and Chemical Evolution of Galaxies. Camridge Univ. Press, Cambridge
Pasquali A., Gallazzi A., Fontanot F., van den Bosch F. C., De Lucia G., Mo H. J., Yang X., 2010, MNRAS, 407, 937
Peng Y., Maiolino R., Cochrane R., 2015, Nature, 521, 192
Peng Y.-j., Maiolino R., 2014, MNRAS, 443, 3643
Pérez-Montero E., 2014, MNRAS, 441, 2663
Pérez-Montero E., Contini T., 2009, MNRAS, 398, 949
Pérez-Montero E. et al., 2013, A&A, 549, A25
Pettini M., Shapley A. E., Steidel C. C., Cuby J.-G., Dickinson M., Moorwood A. F. M., Adelberger K. L., Giavalisco M., 2001, ApJ, 554, 981

Pettini M., Ellison S. L., Bergeron J., Petitjean P., 2002, A&A, 391, 21
Pettini M., Zych B. J., Steidel C. C., Chaffee F. H., 2008, MNRAS, 385, 2011
Pilyugin L. S., 1993, A&A, 277, 42
Pilyugin L. S., Vílchez J. M., Thuan T. X., 2010, ApJ, 720, 1738
Pipino A., Matteucci F., 2004, MNRAS, 347, 968
Prochaska J. X., Wolfe A. M., 2009, ApJ, 696, 1543
Putman M. E., Peek J. E. G., Joung M. R., 2012, ARA&A, 50, 491
Recchi S., Matteucci F., D'Ercole A., 2001, MNRAS, 322, 800
Recchi S., Spitoni E., Matteucci F., Lanfranchi G. A., 2008, A&A, 489, 555
Renzini A., Voli M., 1981, A&A, 94, 175
Romano D., Karakas A. I., Tosi M., Matteucci F., 2010, A&A, 522, A32
Salpeter E. E., 1955, ApJ, 121, 161
Sánchez S. F. et al., 2015, A&A, 574, A47
Schmidt M., 1963, ApJ, 137, 758
Thomas D., Maraston C., Bender R., Mendes de Oliveira C., 2005, ApJ, 621, 673
Thomas D., Maraston C., Schawinski K., Sarzi M., Silk J., 2010, MNRAS, 404, 1775
Thuan T. X., Izotov Y. I., Lipovetsky V. A., 1995, ApJ, 445, 108
Tinsley B. M., 1979, ApJ, 229, 1046
Tinsley B. M., 1980, Fundam. Cosm. Phys., 5, 287
Tremonti C. A. et al., 2004, ApJ, 613, 898
van de Voort F., Schaye J., Booth C. M., Haas M. R., Dalla Vecchia C., 2011, MNRAS, 414, 2458
van den Bergh S., 1962, AJ, 67, 486
Veilleux S., Osterbrock D. E., 1987, ApJ, 63, 295
Ventura P., D'Antona F., 2009, A&A, 499, 835
Ventura P., Zeppieri A., Mazzitelli I., D'Antona F., 1998, A&A, 334, 953
Ventura P., Di Criscienzo M., Carini R., D'Antona F., 2013, MNRAS, 431, 3642
Vila-Costas M. B., Edmunds M. G., 1992, MNRAS, 259, 121
Vincenzo F., Matteucci F., Belfiore F., Maiolino R., 2016, MNRAS, 455, 4183
Wang B., 1991, ApJ, 374, 456
Whittet D. C. B., 2003, Dust in the Galactic Environment, 2nd edn. IoP Publishing, Bristol
Whittet D. C. B., 2010, ApJ, 710, 1009
York D. G. et al., 2000, AJ, 120, 1579

This paper has been typeset from a TEX/LATEX file prepared by the author.